Inorg. Chem. **2002**, *41*, 827–837

Synthetic Analogue of the $\{Fe_2(\mu\text{-}OH)_2(\mu\text{-}O_2CR)\}^{3+}$ Core of Soluble Methane Monooxygenase Hydroxylase via Synthesis and Dioxygen Reactivity of Carboxylate-Bridged Diiron(II) Complexes

Dongwhan Lee and Stephen J. Lippard*

Contribution from the Department of Chemistry, Massachusetts Institute of Technology, Cambridge, Massachusetts 02139

Received September 26, 2001

We describe the synthesis and dioxygen reactivity of diiron(II) tetracarboxylate complexes $[Fe_2(\mu\text{-}O_2CAr^{Tol})_2(O_2CAr^{Tol})_2(N,N\text{-}Me_2en)_2]$ (**2**) and $[Fe_2(\mu\text{-}O_2CAr^{Tol})_2(O_2CAr^{Tol})_2(N,N\text{-}Bn_2en)_2]$ (**6**), where $Ar^{Tol}CO_2^- =$ 2,6-di(*p*-tolyl)benzoate. These complexes were prepared as models for the diiron(II) center in the hydroxylase component of soluble methane monooxygenase (MMOH). Compound **6** reacts with dioxygen to afford PhCHO in ~60(5)% yield, following oxidative N-dealkylation of the pendant benzyl group on the diamine ligand. The diiron(III) complex $[Fe_2(\mu\text{-}OH)_2(\mu\text{-}O_2CAr^{Tol})(O_2CAr^{Tol})_3(N\text{-}Bnen)(N,N\text{-}Bn_2en)]$ (**8**) was isolated from the reaction mixture. The 4.2 K Mössbauer spectrum of **8** displays a single quadrupole doublet with parameters $\delta = 0.48(2)$ mm s^{-1} and $\Delta E_Q = 0.61(2)$ mm s^{-1}. The $\{Fe_2(\mu\text{-}OH)_2(\mu\text{-}O_2CR)\}^{3+}$ core structure in **8** matches that of the fully oxidized form of MMOH. The conversion of **6** to **8** closely parallels the chemistry of MMOH in which an O_2-derived oxygen atom is inserted into the C–H bond of methane. Several reaction pathways are considered to account for this novel chemical transformation, and these are compared with mechanistic frameworks previously developed for related cytochrome P450 and copper(I) dioxygen chemistry.

Introduction

The selective oxidation of hydrocarbons under ambient conditions is a formidable synthetic task.[1] Certain iron(II)[2] and copper(I)[3] centers in biological systems use dioxygen to effect the controlled two-electron oxidation of organic substrates. Chemical strategies adopted by these metalloenzymes for the transfer of metal-bound, dioxygen-derived units to the C−H bonds have attracted considerable scientific interest and engendered an active research area in bioinorganic chemistry.[4−8] Recent progress in detailing the oxo transfer steps in cytochrome P450 (cP450) enzymes[2d,9] and their synthetic analogues[10−13] exemplify how such endeavors can be rewarded by complementary approaches.

The hydroxylase component of methane monooxygenase (MMOH) houses carboxylate-bridged non-heme diiron cen-

* Corresponding author. E-mail: lippard@lippard.mit.edu.

(1) (a) Shilov, A. E.; Shul'pin, G. B. *Chem. Rev.* **1997**, *97*, 2879. (b) Stahl, S. S.; Labinger, J. A.; Bercaw, J. E. *Angew. Chem., Int. Ed.* **1998**, *37*, 2180. (c) Shilov, A. E.; Shteinman, A. A. *Acc. Chem. Res.* **1999**, *32*, 763.
(2) (a) Feig, A. L.; Lippard, S. J. *Chem. Rev.* **1994**, *94*, 759. (b) Que, L., Jr.; Ho, R. Y. N. *Chem. Rev.* **1996**, *96*, 2607. (c) Wallar, B. J.; Lipscomb, J. D. *Chem. Rev.* **1996**, *96*, 2625. (d) Sono, M.; Roach, M. P.; Coulter, E. D.; Dawson, J. H. *Chem. Rev.* **1996**, *96*, 2841. (e) Solomon, E. I.; Brunold, T. C.; Davis, M. I.; Kemsley, J. N.; Lee, S.-K.; Lehnert, N.; Neese, F.; Skulan, A. J.; Yang, Y.-S.; Zhou, J. *Chem. Rev.* **2000**, *100*, 235.
(3) (a) *Bioinorganic Chemistry of Copper*; Karlin, K. D., Tyeklár, Z., Eds.; Chapman & Hall: New York, 1993. (b) Solomon, E. I.; Sundaram, U. M.; Machonkin, T. E. *Chem. Rev.* **1996**, *96*, 2563.
(4) Tolman, W. B. *Acc. Chem. Res.* **1997**, *30*, 227.
(5) Liang, H.-C.; Dahan, M.; Karlin, K. D. *Curr. Opin. Chem. Biol.* **1999**, *3*, 168.
(6) Mahadevan, V.; Klein Gebbink, R. J. M.; Stack, T. D. P. *Curr. Opin. Chem. Biol.* **2000**, *4*, 228.
(7) Du Bois, J.; Mizoguchi, T. J.; Lippard, S. J. *Coord. Chem. Rev.* **2000**, *200−202*, 443.
(8) Tolman, W. B.; Spencer, D. J. E. *Curr. Opin. Chem. Biol.* **2001**, *5*, 188.
(9) (a) Newcomb, M.; Toy, P. H. *Acc. Chem. Res.* **2000**, *33*, 449. (b) Hata, M.; Hirano, Y.; Hoshino, T.; Tsuda, M. *J. Am. Chem. Soc.* **2001**, *123*, 6410.
(10) (a) Lee, K. A.; Nam, W. *J. Am. Chem. Soc.* **1997**, *119*, 1916. (b) Goh, Y. M.; Nam, W. *Inorg. Chem.* **1999**, *38*, 914. (c) Nam, W.; Lim, M. H.; Lee, H. J.; Kim, C. *J. Am. Chem. Soc.* **2000**, *122*, 6641. (d) Nam, W.; Han, H. J.; Oh, S.-Y.; Lee, Y. J.; Choi, M.-H.; Han, S.-Y.; Kim, C.; Woo, S. K.; Shin, W. *J. Am. Chem. Soc.* **2000**, *122*, 8677. (e) Nam, W.; Lim, M. H.; Moon, S. K.; Kim, C. *J. Am. Chem. Soc.* **2000**, *122*, 10805.
(11) Bernadou, J.; Meunier, B. *Chem. Commun.* **1998**, 2167.
(12) Collman, J. P.; Chien, A. S.; Eberspacher, T. A.; Brauman, J. I. *J. Am. Chem. Soc.* **2000**, *122*, 11098.
(13) Woggon, W.-D.; Wagenknecht, H.-A.; Claude, C. *J. Inorg. Biochem.* **2001**, *83*, 289.

10.1021/ic011008s CCC: $22.00
Published on Web 01/31/2002

ters that bind and activate dioxygen.[2a,c,e,14,15] Cleavage of a metal-bound O−O bond affords a highly reactive di(μ-oxo)-diiron(IV) species $MMOH_Q$[16] that can insert one oxygen atom into C−H bonds of various substrates, including CH_4. The reaction coordinates traversed by the enzyme intermediates have been predominantly probed by direct biological studies on MMOH itself[14,16,17] and further evaluated by DFT calculations.[18−22] Parallel progress in non-heme iron-modeling chemistry has been hampered, however, by the scarcity of enzyme analogues that integrate biomimetic structural and functional properties into a single system.[7] Mechanistic information obtained by well-defined low molecular weight analogues can be used to calibrate the geometric and electronic parameters involved in key O−O and C−H bond activation steps of the MMOH reaction cycle.

For some time, we[23−25] and others[26,27] have been exploring the chemistry of non-heme diiron complexes supported by *m*-terphenyl-derived carboxylate ligands. Key architectural features of the carboxylate-rich enzyme active sites have been faithfully reproduced in such constructs,[23,26] some of which display biomimetic O_2 reactivity properties.[24,26] Depending on the choice of carboxylate ligands, either (peroxo)diiron-(III)[26] or high-valent iron(III)iron(IV)[24] species were accessed. Effective steric shielding provided by the aryl moieties apparently prevents deleterious bimolecular decompositions of the highly reactive dioxygen adduct(s) encapsulated therein.

During our investigation of the $Ar^{Tol}CO_2^-$-based model system, we realized that some of the oxidizing equivalents of the dioxygen adduct(s) were being quenched by electron transfer (ET) from the diiron(II) precursor compound (Scheme 1).[24] According to this mechanistic model, **A** is the major isomer in equilibrium with **B** for the $[Fe_2(\mu\text{-}O_2CAr^{Tol})_4L_2]$ (L = pyridine derivatives) system at low temperature. The oxygenation reaction is slow, presumably because it requires

Scheme 1

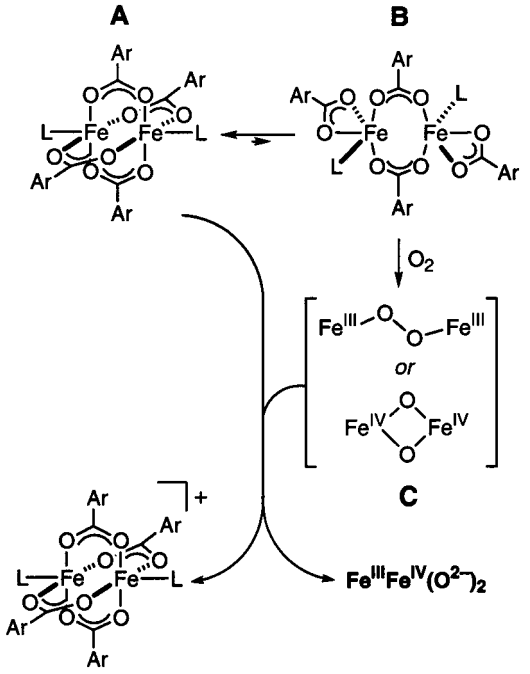

A to **B** conversion via carboxylate shifts.[28] Under these conditions, the putative initial O_2 adduct(s) **C** is rapidly reduced by **A**, affording a mixture of Fe(III)Fe(IV) and Fe(II)Fe(III) species as the products. Overlap between the redox windows of **A** and **C** facilitates this unwanted ET process.

To generate significant quantities of functionally competent high-valent diiron(IV) oxo species, we reasoned that it would be advantageous if the reactive isomer **B** were predominant in solution. Rapid reaction of **B** with dioxygen would prevent the quenching of oxidizing equivalents in **C**. To achieve this goal, we implemented two different synthetic strategies, as depicted in Scheme 2. In one, the *m*-terphenyl ligand fragment is laterally expanded (**I**, Scheme 2), enhancing interligand steric crowding and thus destabilizing the quadruply bridged core in **A**. Alternatively, the doubly bridged isomer (**B′**) is accessed by installing a bidentate ligand at each iron atom (**II**, Scheme 2). In the latter case, the six-coordinate isomer **A′** adopts a highly strained coordination geometry that introduces a significant degree of steric crowding at the axial positions. Strategy **I** did not lead to the desired results. Instead, reactivity patterns similar to that depicted in Scheme 1 were observed,[29] or higher nuclearity iron(II) complexes were obtained.[30] Strategy **II** was successfully implemented, however.

In particular, $[Fe_2(\mu\text{-}O_2CAr^{Tol})_2(O_2CAr^{Tol})_2(N,N\text{-}Bn_2en)_2]$ (**6**) reacts with dioxygen to afford the diiron(III) complex $[Fe_2(\mu\text{-}OH)_2(\mu\text{-}O_2CAr^{Tol})(O_2CAr^{Tol})_3(N\text{-}Bnen)(N,N\text{-}Bn_2en)]$ (**8**).[31] This chemistry closely parallels the activation of dioxygen by non-heme diiron enzymes and is analogous to

(14) Merkx, M.; Kopp, D. A.; Sazinsky, M. H.; Blazyk, J. L.; Müller, J.; Lippard, S. J. *Angew. Chem., Int. Ed.* **2001**, *40*, 2782.
(15) Whittington, D. A.; Lippard, S. J. In *Handbook of Metalloproteins*; Messerschmidt, A., Huber, R., Poulos, T., Wieghardt, K., Eds.; Wiley & Sons: Chichester, 2001; pp 712−724.
(16) (a) Lee, S.-K.; Fox, B. G.; Froland, W. A.; Lipscomb, J. D.; Münck, E. *J. Am. Chem. Soc.* **1993**, *115*, 6450. (b) Liu, K. E.; Valentine, A. M.; Wang, D.; Huynh, B. H.; Edmondson, D. E.; Salifoglou, A.; Lippard, S. J. *J. Am. Chem. Soc.* **1995**, *117*, 10174. (c) Shu, L.; Nesheim, J. C.; Kauffmann, K.; Münck, E.; Lipscomb, J. D.; Que, L., Jr. *Science* **1997**, *275*, 515.
(17) Valentine, A. M.; Stahl, S. S.; Lippard, S. J. *J. Am. Chem. Soc.* **1999**, *121*, 3876.
(18) Siegbahn, P. E. M.; Crabtree, R. H. *J. Am. Chem. Soc.* **1997**, *119*, 3103.
(19) Siegbahn, P. E. M. *Inorg. Chem.* **1999**, *38*, 2880.
(20) Dunietz, B. D.; Beachy, M. D.; Cao, Y.; Whittington, D. A.; Lippard, S. J.; Friesner, R. A. *J. Am. Chem. Soc.* **2000**, *122*, 2828.
(21) Gherman, B. J.; Dunietz, B. D.; Whittington, D. A.; Lippard, S. J.; Friesner, R. A. *J. Am. Chem. Soc.* **2001**, *123*, 3836.
(22) Friesner, R. A.; Dunietz, B. D. *Acc. Chem. Res.* **2001**, *34*, 351.
(23) Lee, D.; Lippard, S. J. *J. Am. Chem. Soc.* **1998**, *120*, 12153.
(24) Lee, D.; Du Bois, J.; Petasis, D.; Hendrich, M. P.; Krebs, C.; Huynh, B. H.; Lippard, S. J. *J. Am. Chem. Soc.* **1999**, *121*, 9893.
(25) Lee, D.; Krebs, C.; Huynh, B. H.; Hendrich, M. P.; Lippard, S. J. *J. Am. Chem. Soc.* **2000**, *122*, 5000.
(26) Hagadorn, J. R.; Que, L., Jr.; Tolman, W. B. *J. Am. Chem. Soc.* **1998**, *120*, 13531.
(27) Hagadorn, J. R.; Que, L., Jr.; Tolman, W. B.; Prisecaru, I.; Münck, E. *J. Am. Chem. Soc.* **1999**, *121*, 9760.
(28) Rardin, R. L.; Tolman, W. B.; Lippard, S. J. *New J. Chem.* **1991**, *15*, 417.
(29) Lee, D.; Lippard, S. J. Unpublished results.
(30) Lee, D.; Sorace, L.; Caneschi, A.; Lippard, S. J. *Inorg. Chem.* **2001**, *40*, 6774.

Scheme 2

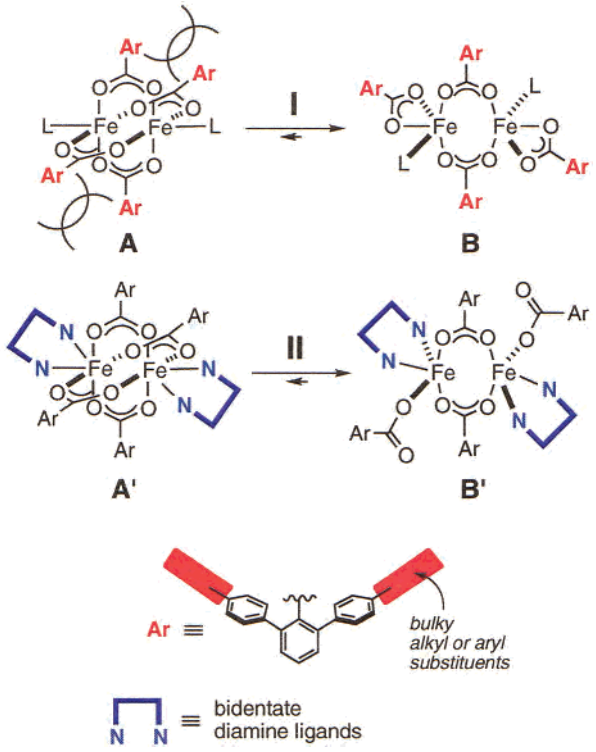

the dealkylation of heteroatom-containing substrates effected by cP450.[2] A consequence of this biomimetic oxidative N-dealkylation was the synthesis of the long-sought structural model of the diiron core in $MMOH_{ox}$.[31] In this contribution, we report full details of this chemistry as well as the synthesis and characterization of the carboxylate-bridged diiron(II) precursor complexes. Collectively, these findings represent a significant expansion in the scope of structural and reactivity properties of non-heme diiron model compounds. Aspects of this work have been previously communicated.[32]

Experimental Section

General Considerations. All reagents were obtained from commercial suppliers and used as received, unless otherwise noted. Dichloromethane and acetonitrile were distilled over CaH_2 under nitrogen. Diethyl ether, pentanes, and THF were saturated with nitrogen and purified by passage through activated Al_2O_3 columns under nitrogen.[33] Dioxygen (99.994%, BOC Gases) was dried by passing the gas stream through a column of Drierite. ^{18}O-enriched dioxygen (99%) was supplied by ICON, NY. The compounds $Fe(OTf)_2$·2MeCN,[34] 2,6-di(*p*-tolyl)benzoic acid ($Ar^{Tol}CO_2H$),[35] 2,6-di(4-fluorophenyl)benzoic acid ($Ar^{4\text{-}FPh}CO_2H$),[35] 2,6-di(4-*tert*-butylphenyl)benzoic acid ($Ar^{4\text{-}tBuPh}CO_2H$),[30] *N*,*N*-dibenzylethylenediamine (*N*,*N*-Bn_2en),[36,37] and *N*,*N*-dibenzylpropylamine[38] were prepared as described in the literature. The synthesis and characterization of the compounds $[Fe_2(\mu\text{-}O_2CAr^{Tol})_2(O_2CAr^{Tol})_2(THF)_2]$ (**1**)[23] and $[Fe_2(\mu\text{-}O_2CAr^{Tol})_4(4\text{-}^tBuC_5H_4N)_2]$[24] have been reported. The sodium salts of the carboxylic acids, NaO_2CAr^{Tol}, $NaO_2CAr^{4\text{-}FPh}$, and $NaO_2CAr^{4\text{-}tBuPh}$, were prepared by treating a MeOH solution of the free acid with 1 equiv of NaOH and removing the volatile fractions under reduced pressure. Air-sensitive manipulations were carried out under nitrogen in a Vacuum Atmospheres drybox or by standard Schlenk line techniques.

Physical Measurements. FT-IR spectra were recorded on a Bio-Rad FTS-135 instrument with WIN-IR software. UV−vis spectra were recorded on a Hewlett-Packard 8453 diode array spectrophotometer. Mössbauer spectra were obtained on an MS1 spectrometer (WEB Research Co.) with a ^{57}Co source in a Rh matrix maintained at room temperature in the MIT Department of Chemistry Instrumentation Facility. Solid samples were prepared by suspending ~0.015 mmol of the powdered material in Apeizon N grease and packing the mixture into a nylon sample holder. All data were collected at 4.2 K, and the isomer shift (δ) values are reported with respect to natural iron foil that was used for velocity calibration at room temperature. The spectra were fit to Lorentzian lines by using the *WMOSS* plot and fit program.[39]

$[Fe_2(\mu\text{-}O_2CAr^{Tol})_2(O_2CAr^{Tol})_2(N,N\text{-}Me_2en)_2]$ (2), $[Fe_2(\mu\text{-}O_2CAr^{Tol})_3(O_2CAr^{Tol})(N,N\text{-}Me_2en)]$ (3) and $[Fe(O_2CAr^{Tol})_2(N,N\text{-}Me_2en)_2]$ (4). To a rapidly stirred CH_2Cl_2 (4 mL) solution of **1** (181 mg, 0.124 mmol) was added dropwise neat *N*,*N*-Me_2en[31] (27 μL, 0.25 mmol). The pale yellow reaction mixture was stirred for 0.5 h, mixed with PhCl (1 mL), and layered with pentanes. Pale yellow blocks (87 mg, 47% based on **1**) deposited within a few days and were analyzed by X-ray crystallography. Repeated attempts to isolate analytically pure **2** were not successful. The major contaminants included **3** and **4**, as judged by crystallographic chemical analysis.

$[Fe_2(\mu\text{-}O_2CAr^{4\text{-}tBuPh})_2(OTf)_2(N,N\text{-}Bn_2en)_2]$ (5). To a rapidly stirred MeCN (10 mL) solution of $Fe(OTf)_2$·2MeCN (218 mg, 0.500 mmol) was added a single portion of $NaO_2CAr^{4\text{-}tBuPh}$ (210 mg, 0.514 mmol). The reaction mixture clarified within a few minutes. A portion of neat *N*,*N*-Bn_2en (120 mg, 0.500 mmol) was added dropwise, and the resulting pale yellow solution was stirred for 2 h. Volatile fractions were removed, and the off-white residual solid material was extracted into CH_2Cl_2 (20 mL). Insoluble material was filtered off, and the filtrate was concentrated to ca. 10 mL. Vapor diffusion of pentanes into the filtrate afforded colorless blocks of **5** (165 mg, 99.3 μmol, 40%), which were suitable for X-ray crystallography. FT-IR (KBr, cm^{-1}): 3337, 3323, 3276, 2966, 2905, 2870, 1593, 1568, 1456, 1389, 1317, 1240, 1220, 1169, 1032, 849, 752, 703, 635, 578. Anal. Calcd for $C_{88}H_{98}N_4O_{10}F_6Fe_2S_2$: C, 63.61; H, 5.94; N, 3.37. Found: C, 63.57; H, 5.89; N, 3.37.

$[Fe_2(\mu\text{-}O_2CAr^{Tol})_2(O_2CAr^{Tol})_2(N,N\text{-}Bn_2en)_2]$ (6). To a rapidly stirred yellow CH_2Cl_2 solution (10 mL) of **1** (505 mg, 0.346 mmol) was added dropwise neat *N*,*N*-Bn_2en (166 mg, 0.691 mmol). The resulting pale yellow solution was stirred for 10 min and filtered through Celite. Pale yellow blocks of **6** (608 mg, 98%), suitable for X-ray crystallography, were obtained by vapor diffusion of pentanes/hexanes (1:1) into the filtrate. FT-IR (KBr, cm^{-1}): 3324,

(31) Abbreviations used: $Ar^{Tol}CO_2^-$, 2,6-di(*p*-tolyl)benzoate; $Ar^{Mes}CO_2^-$, 2,6-dimesitylbenzoate; $MMOH_{ox}$, MMOH in the iron(III)/iron(III) oxidation states; $MMOH_{red}$, MMOH in the iron(II)/iron(II) oxidation states; *N*,*N*-Bn_2en, *N*,*N*-dibenzylethylenediamine; *N*,*N*-Me_2en, *N*,*N*-dimethylethylenediamine; *N*-Bnen, *N*-benzylethylenediamine; L^1, *N*,*N*′-bis(pyridin-2-ylmethyl)-*N*,*N*″-bis(3,4,5-trimethoxybenzyl)ethane-1,2-diamine; TMEDA, *N*,*N*,*N*′,*N*′-tetramethylethylenediamine

(32) Lee, D.; Lippard, S. J. *J. Am. Chem. Soc.* **2001**, *123*, 4611.

(33) Pangborn, A. B.; Giardello, M. A.; Grubbs, R. H.; Rosen, R. K.; Timmers, F. J. *Organometallics* **1996**, *15*, 1518.

(34) Hagen, K. S. *Inorg. Chem.* **2000**, *39*, 5867.

(35) (a) Du, C.-J. F.; Hart, H.; Ng, K.-K. D. *J. Org. Chem.* **1986**, *51*, 3162. (b) Saednya, A.; Hart, H. *Synthesis* **1996**, 1455. (c) Chen, C.-T.; Siegel, J. S. *J. Am. Chem. Soc.* **1994**, *116*, 5959.

(36) Guillaume, D.; Aitken, D. J.; Husson, H.-P. *Synlett* **1991**, 747.

(37) Iwanami, S.; Takashima, M.; Hirata, Y.; Hasegawa, O.; Usuda, S. *J. Med. Chem.* **1981**, *24*, 1224.

(38) Trapani, G.; Reho, A.; Latrofa, A. *Synthesis* **1983**, 1013.

(39) Kent, T. A. *WMOSS : Mössbauer Spectral Analysis Software*, version 2.5; WEB Research Company: Minneapolis, MN, 1998.

Table 1. Summary of X-ray Crystallographic Data

	5	**6**	**7**·CH_2Cl_2	**8**·2PhCl·0.5C_5H_{12}
formula	$C_{88}H_{96}N_4O_{10}F_6S_2Fe_2$	$C_{116}H_{104}N_4O_8Fe_2$	$C_{109}H_{80}N_4O_8Cl_2F_8Fe_2$	$C_{123.5}H_{109}N_4O_{10}Cl_2Fe_2$
fw, g/mol	1659.51	1793.73	1908.37	1991.75
space group	$P2_1/c$	$P\bar{1}$	$P2_1/n$	$P\bar{1}$
a, Å	11.7193(3)	11.3953(5)	13.7575(0)	15.0043(18)
b, Å	19.4414(5)	14.7207(7)	21.0669(5)	16.907(2)
c, Å	18.3893(3)	15.2957(7)	17.7305(4)	24.019(3)
α, deg		77.8360(10)		95.570(2)
β, deg	101.6710(10)	72.1730(10)	99.2350(10)	108.017(2)
γ, deg		82.1620(10)		104.939(2)
V, Å^3	4103.19(16)	2380.64(19)	5072.19(17)	5493.8(11)
Z	2	1	2	2
ρ_{calc}, g/cm^3	1.343	1.251	1.250	1.204
T, °C	−85	−85	−85	−85
μ (Mo Kα), mm^{-1}	0.479	0.366	0.410	0.372
θ limits, deg	1.77−28.31	1.82−28.28	1.51−28.27	1.64−28.26
total no. of data points	30 462	15 061	31 670	48 676
no. of unique data points	9480	10 469	11 783	24 430
no. of parameters	513	608	611	1241
R (%)[a]	4.38	5.53	7.23	5.46
R_w^2 (%)[b]	10.18	11.84	21.16	15.70
max, min peaks, e/Å^3	0.734, −0.580	0.435, −0.397	1.188, −0.698	0.866, −0.905

[a] $R = \Sigma||F_o| - |F_c||/\Sigma|F_o|$. [b] $R_w^2 = \{\Sigma[w(F_o^2 - F_c^2)^2]/\Sigma[w(F_o^2)^2]\}^{1/2}$.

3261, 3052, 3024, 2919, 2794, 1605, 1561, 1515, 1494, 1454, 1410, 1383, 1307, 1268, 1187, 1146, 1110, 1170, 1044, 1020, 977, 855, 820, 801, 784, 765, 748, 736, 701, 584, 544, 521. Anal. Calcd for $C_{116}H_{108}N_4O_8Fe_2$: C, 77.50; H, 6.05; N, 3.12. Found: C, 77.22; H, 6.35; N, 3.08.

[Fe$_2$(μ-O$_2$CAr$^{4\text{-FPh}}$)$_2$(O$_2$CAr$^{4\text{-FPh}}$)$_2$(*N*,*N*-Bn$_2$en)$_2$] (7). To a rapidly stirred THF (10 mL) solution of Fe(OTf)$_2$·2MeCN (220 mg, 0.504 mmol) was added dropwise neat *N*,*N*-Bn$_2$en (132 μL, 0.498 mmol). A portion of NaO$_2$CAr$^{4\text{-FPh}}$ (340 mg, 1.02 mmol) was added, and the heterogeneous mixture was stirred overnight to afford a pale yellow, clear solution. Volatile fractions were removed, and the residual pale yellow solid was extracted into CH_2Cl_2 (7 mL). Insoluble material was filtered off. Vapor diffusion of Et_2O into the filtrate afforded pale yellow blocks of **7** (350 mg, 97%), which were suitable for X-ray crystallography. FT-IR (KBr, cm^{-1}): 3324, 3062, 2800, 1606, 1576, 1545, 1512, 1454, 1405, 1382, 1225, 1160, 1117, 1095, 1070, 843, 810, 792, 773, 750, 701, 555, 532. Anal. Calcd for $C_{108}H_{84}N_4O_8F_8Fe_2$: C, 70.90; H, 4.63; N, 3.06. Found: C, 70.52; H, 4.57; N, 3.06.

[Fe$_2$(μ-OH)$_2$(μ-O$_2$CAr$^{\text{Tol}}$)(O$_2$CAr$^{\text{Tol}}$)$_3$(*N*-Bnen)(*N*,*N*-Bn$_2$en)] (8)[31]. A CH_2Cl_2 solution (10 mL) of **6** (355 mg, 0.195 mmol) was saturated with dry dioxygen at room temperature over a period of 10 min. The dark brown solution was filtered through Celite, concentrated to ca. 5 mL, and layered with pentanes at room temperature. Bright yellow blocks of **8** (166 mg, 95.3 μmol, 49%) were obtained within several days. Yellow blocks of **8**·2PhCl·0.5C_5H_{12}, suitable for X-ray crystallography, were obtained by layering pentanes over a saturated PhCl solution of this material at room temperature. FT-IR (KBr, cm^{-1}): 3579, 3328, 3275, 3057, 3025, 2920, 1607, 1543, 1515, 1495, 1454, 1407, 1337, 1186, 1144, 1110, 1070, 1021, 1002, 820, 801, 785, 766, 738, 699, 608, 584, 546, 526, 449. Anal. Calcd for $C_{109}H_{104}N_4O_{10}Fe_2$: C, 75.17; H, 6.02; N, 3.22. Found: C, 75.30; H, 6.03; N, 3.10.

X-ray Crystallographic Studies. Intensity data were collected on a Bruker (formerly Siemens) CCD diffractometer with graphite-monochromated Mo Kα radiation (λ = 0.71073 Å) controlled by a Pentium-based PC running the *SMART* software package.[40] Single crystals were mounted at room temperature on the tips of quartz fibers, coated with Paratone-N oil, and cooled to 188 K under a stream of cold nitrogen maintained by a Bruker LT-2A nitrogen cryostat. Data collection and reduction protocols are described elsewhere.[41] The structures were solved by direct methods and refined on F^2 by using the *SHELXTL* software package.[42] Empirical absorption corrections were applied with *SADABS*,[43] which is part of the *SHELXTL* program package, and the structures were checked for higher symmetry by using the program *PLATON*.[44] All non-hydrogen atoms were refined anisotropically unless otherwise noted. In general, hydrogen atoms were assigned idealized positions and given thermal parameters equivalent to either 1.5 (methyl hydrogen atoms) or 1.2 (all other hydrogen atoms) times the thermal parameter of the carbon atom to which they were attached. The hydrogen atoms associated with the following groups were located in the difference Fourier maps and refined isotropically: NH_2 groups on **2**−**8**, the NH group on **8**, and OH groups on **8**. Hydrogen atoms bound to disordered solvent molecules were not included in the refinement. The structure of **2** contains a disordered CH_2Cl_2 molecule that was distributed over three positions and refined isotropically at occupancies of 0.5, 0.35, and 0.15. The carbon atom α to the primary amine of the *N*,*N*-Bn$_2$en ligand in **6** was distributed over two positions and refined anisotropically at occupancies of 0.75 and 0.25. A disordered CH_2Cl_2 molecule in the structure of **7** was equally distributed over two positions and refined isotropically. The lattice solvent molecules in the structure of **8** were modeled as pentane and chlorobenzene. Crystallographic information is provided in Table 1.

General Procedures for Amine N-Dealkylation Studies. Samples (~12 mM [Fe$_2$] dissolved in 1.0 mL of CH_2Cl_2) were prepared in the drybox and loaded into a 6 mL glass vial sealed with a rubber septum. For external substrate oxidation studies, *N*,*N*-dibenzylpropylamine (1 equiv with respect to one iron(II) center) was added to the solution. The sample was brought out of the drybox and gently purged with dry O_2 at atmospheric pressure for

(40) *SMART: Software for the CCD Detector System*, version 5.05; Bruker AXS: Madison, WI, 1998.

(41) Feig, A. L.; Bautista, M. T.; Lippard, S. J. *Inorg. Chem.* **1996**, *35*, 6892.

(42) Sheldrick, G. M. *SHELXTL97-2: Program for the Refinement of Crystal Structures*; University of Göttingen, Germany, 1997.

(43) Sheldrick, G. M. *SADABS: Area-Detector Absorption Correction*; University of Göttingen, Germany, 1996.

(44) Spek, A. L. *PLATON: A Multipurpose Crystallographic Tool*; Utrecht University: Utrecht, The Netherlands, 1998.

5 min with constant stirring. The resulting oxidation mixture was allowed to stir for 0.5 h, and a CH_2Cl_2 solution of 1,2-dichlorobenzene was added as an internal standard. The mixture was filtered through silica gel (0.5 cm × 1.0 cm), and the filter cake was washed with additional CH_2Cl_2 (2 mL). The combined filtrates were analyzed by GC. No significant changes were observed in the relative amounts of the PhCHO product and internal standard before and after filtration through the silica plug.

GC Analyses. Analyses were carried out on a Hewlett-Packard HP-5970 gas chromatograph connected to a HP-5971 mass analyzer. An Alltech Econo-cap EC-WAX capillary column (30 m × 0.25 mm × 0.25 μm) was used for GC/MS studies. A HP-5 cross-linked 5% PhMe−silicone column (25 m × 0.32 mm × 0.5 μm) was used for GC studies. The following program was used to effect all separations: initial temperature = 50 °C, initial time = 10 min, and a temperature ramp of 50−200 °C at 5 °C/min. The product, benzaldehyde, was identified by comparing its retention time and mass spectral pattern to those of an authentic standard. Coinjection with the authentic sample confirmed the assignment. Integrations were acquired by FID detection with a HP-3393 integrator. Quantitative analysis was performed by comparison with the 1,2-dichlorobenzene internal standard. Calibration plots for the detector response were prepared for benzaldehyde and 1,2-dichlorobenzene by using stock solutions of known concentrations.

Isotope-Labeling Experiments. A colorless CH_2Cl_2 (2.5 mL) solution of **6** (41 mg) was loaded into a Teflon screw-capped Schlenk flask. The sample was degassed by three successive freeze−pump−thaw cycles and placed in a liquid N_2 bath. The headspace was evacuated on a vacuum line, and $^{18}O_2$ was vacuum-transferred into the flask. The mixture was allowed to warm to room temperature, resulting in a color change to yellowish green. The reaction mixture was stirred for 0.5 h and analyzed by GC−MS: t_R = 9.9 min and *m*/*z* (abundance) = 108.10 (8068, PhCH^{18}O, M^+), 106.00 (1048, PhCHO, M^+)

Results

Synthesis and Structural Characterization of [Fe_2(μ-O_2CAr^{Tol})$_2$(O_2CAr^{Tol})$_2$(*N*,*N*-Me_2en)$_2$] (2), [Fe_2(μ-O_2CAr^{Tol})$_3$(O_2CAr^{Tol})(*N*,*N*-Me_2en)] (3), and [Fe(O_2CAr^{Tol})$_2$(*N*,*N*-Me_2en)$_2$] (4). Compound **2** was prepared from the reaction of **1** with 2 equiv of *N*,*N*-Me_2en.[31] Colorless blocks were obtained by recrystallization from CH_2Cl_2/PhCl/pentanes and analyzed by X-ray crystallography. The crystal structure of **2** is shown in Figure 1; selected bond lengths and angles are listed in Table 2. Displacement of the weakly bound THF molecules in **1** by the bidentate ligand *N*,*N*-Me_2en induces carboxylate shifts from terminal bidentate to monodentate (Scheme 3) ligands. The alleviation of steric repulsion between the μ-1,3 bridging and terminal carboxylate ligands in **2** is reflected in the significantly reduced metal···metal distance of 3.4245(5) Å compared to 4.2822(7) Å in **1**. Repeated attempts to prepare an analytically pure batch of **2** were unsuccessful. Crystallographic chemical analysis of the reaction batch revealed contamination with the triply bridged dinuclear complex **3** as well as with the mononuclear compound **4**, which was obtained as colorless blocks that were barely distinguishable from **2**. The crystal structures of these compounds are displayed in Figures S1 and S2 (Supporting Information). The Fe···Fe distance of 3.1251(8) Å in **3** is considerably shorter than that in the precursor compound **1**, owing to the presence of the three bridging carboxylate ligands. Bidentate terminal coordination by *N*,*N*-Me_2en and $Ar^{Tol}CO_2^-$ ligands complete the highly distorted trigonal bipyramidal coordination of each iron atom. The tertiary amine group on the chelating *N*,*N*-Me_2en ligand is pointing away from the dimetallic cavity, alleviating inter-ligand steric crowding. The pseudo-octahedral coordination sphere of **4** comprises N_4O_2 donor atom sets contributed by two bidentate diamine and two monodentate carboxylate ligands. The metrical parameters are normal for a high-spin iron(II) complex.

Synthesis and Characterization of [Fe_2(μ-$O_2CAr^{4\text{-}tBuPh}$)$_2$(OTf)$_2$(*N*,*N*-Bn_2en)$_2$] (5), [Fe_2(μ-O_2CAr^{Tol})$_2$(O_2CAr^{Tol})$_2$(*N*,*N*-Bn_2en)$_2$] (6), and [Fe_2(μ-$O_2CAr^{4\text{-}FPh}$)$_2$($O_2CAr^{4\text{-}FPh}$)$_2$(*N*,*N*-Bn_2en)$_2$] (7). Compound **5** was prepared from a

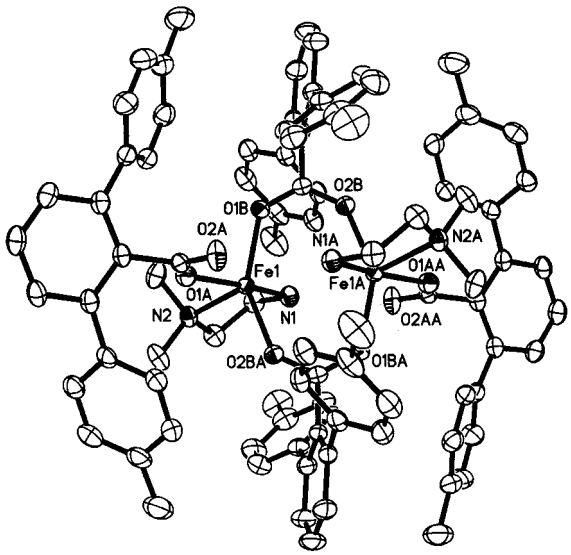

Figure 1. ORTEP diagram of [Fe_2(μ-O_2CAr^{Tol})$_2$(O_2CAr^{Tol})$_2$(*N*,*N*-Me_2en)$_2$] (**2**) with thermal ellipsoids at 50% probability.

Table 2. Selected Bond Lengths and Angles for **2** and **5**−**7**[a]

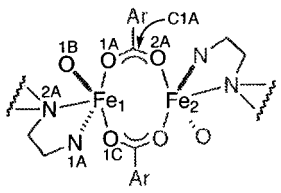

2 and **5**

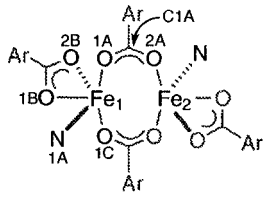

6 and **7**

	2	**5**	**6**	**7**
	Bond Lengths (Å)			
Fe1···Fe2	3.4245(5)	3.8108(6)	4.3598(8)	3.9854(9)
Fe1−O1A	2.0608(13)	2.0062(15)	1.9608(19)	1.913(3)
Fe1−O1C	2.0437(13)	2.0248(15)	2.007(2)	1.981(3)
Fe1−O1B	2.0557(14)	2.1120(17)	2.1060(19)	2.019(2)
Fe1−O2B			2.2131(19)	2.391(2)
Fe1−N1A	2.2068(17)	2.140(2)	2.127(3)	2.124(3)
Fe1−N2A	2.1838(17)	2.2355(18)		
	Bond Angles (deg)			
Fe1−O1A−C1A	129.64(12)	148.53(15)	152.7(2)	155.1(3)
Fe2−O2A−C1A	136.57(12)	127.31(15)	144.8(2)	131.8(3)
N1A−Fe1−N2A	80.36(7)	81.18(7)		

[a] Numbers in parentheses are estimated standard deviations of the last significant figures.

Scheme 3

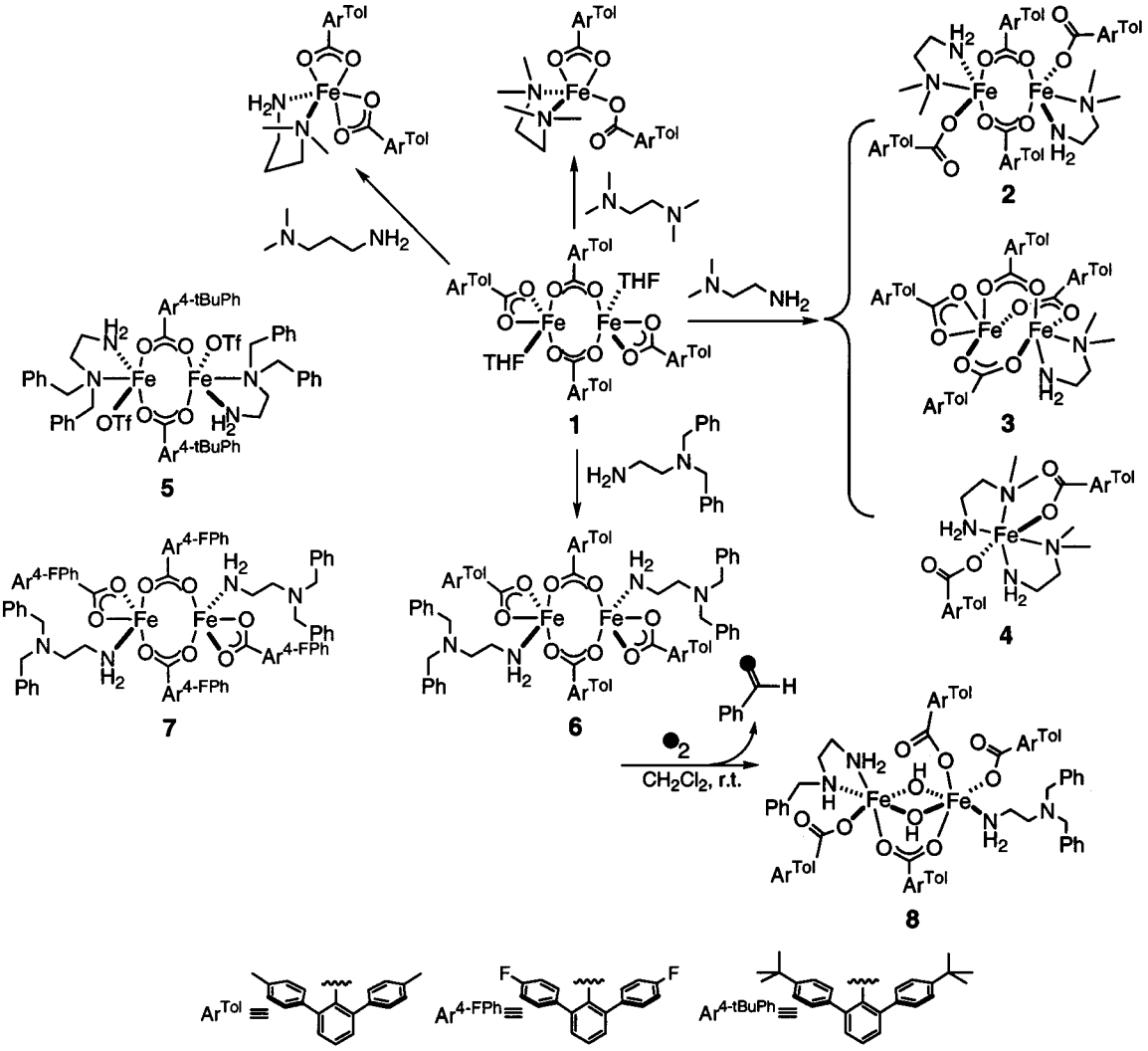

reaction between equimolar amounts of $Fe(OTf)_2 \cdot 2MeCN$, $NaO_2CAr^{4\text{-}tBuPh}$, and *N*,*N*-$Bn_2$en in MeCN. Colorless blocks were obtained in modest yield (~40%) by recrystallization from CH_2Cl_2/pentanes. When similar attempts were made with NaO_2CAr^{Tol}, a highly intractable solid material was obtained after removal of the solvent (THF or MeCN), precluding any further characterization. The crystal structure of **5** is displayed in Figure 2; selected bond lengths and angles are available in Table 2. The five-coordinate iron centers in **5** are related by a crystallographic center of inversion, and a metal···metal distance of 3.8108(6) Å is spanned by two trans-disposed carboxylate ligands. The diamine ligand *N*,*N*-Bn_2en coordinates in bidentate mode in a manner similar to that of *N*,*N*-Me_2en in **2**.

The tetracarboxylate diiron complex **6** was prepared in excellent yield (~98%) via displacement of the THF ligands in **1** by *N*,*N*-Bn_2en. Analytically pure pale yellow blocks were obtained by recrystallization from CH_2Cl_2/pentanes/hexanes. A related compound **7** was conveniently accessed through direct self-assembly from 1:2:1 $Fe(OTf)_2 \cdot 2MeCN/NaO_2CAr^{4\text{-}FPh}$/*N*,*N*-$Bn_2$en. Pale yellow blocks were obtained in excellent yield (~97%) following recrystallization from CH_2Cl_2/Et_2O. The crystal structures of **6** and **7** are shown in Figure 3; selected bond lengths and angles are listed in Table 2. In **6** and **7**, the terminal carboxylates are bidentate, and the diamine ligands *N*,*N*-Bn_2en are monodentate, the opposite of the situation in **2**. The significantly lengthened metal··· metal distances of 4.3598(8) (in **6**) and 3.9854(9) Å (in **7**) compared to that of 3.4245(5) Å in **2** indicates that these

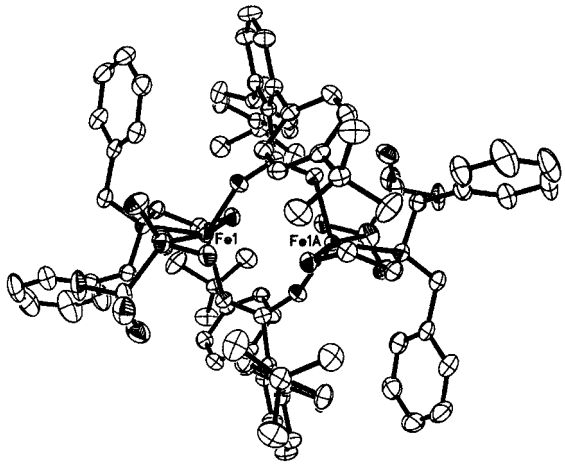

Figure 2. ORTEP diagram of $[Fe_2(\mu\text{-}O_2CAr^{4\text{-}tBuPh})_2(OTf)_2(N,N\text{-}Bn_2en)_2]$ (**5**) with thermal ellipsoids at 50% probability.

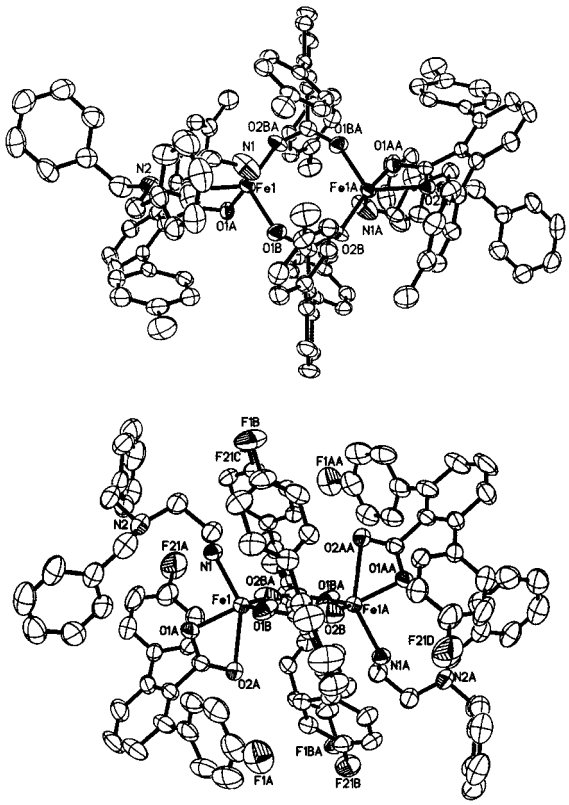

Figure 3. ORTEP diagram of $[Fe_2(\mu\text{-}O_2CAr^{Tol})_2(O_2CAr^{Tol})_2(N,N\text{-}Bn_2en)_2]$ (**6**) (top) and $[Fe_2(\mu\text{-}O_2CAr^{4\text{-}FPh})_2(O_2CAr^{4\text{-}FPh})_2(N,N\text{-}Bn_2en)_2]$ (**7**) (bottom) with thermal ellipsoids at 50% probability.

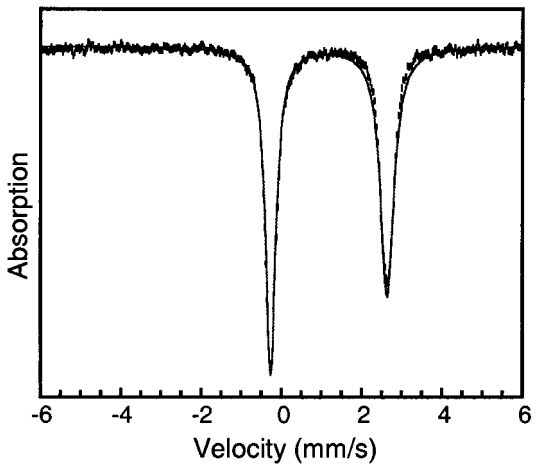

Figure 4. Zero-field Mössbauer spectrum (experimental data (|), calculated fit (−)) recorded at 4.2 K for $[Fe_2(\mu\text{-}O_2CAr^{Tol})_2(O_2CAr^{Tol})_2(N,N\text{-}Bn_2en)_2]$ (**6**) in the solid state. See text for derived Mössbauer parameters.

structural variations arise from steric crowding within the dimetallic core. The binding of the terminal carboxylate ligands is asymmetric, as reflected in the two distinct Fe−O distances with ΔFe−O = 0.11∼0.37 Å (Table 2). The longer Fe−O bonds are positioned trans to the N-donor atoms. The ligand compositions of **6** and **7**, with four carboxylate and two N-donor ligands, are similar to those of related compounds $[Fe_2(\mu\text{-}O_2CAr^{Tol})_2(O_2CAr^{Tol})_2L_2]$, where L = C_5H_5N or 1-MeIm.[23]

Figure 4 displays the 4.2 K zero-field Mössbauer spectrum of **6** in the solid state. The Mössbauer parameters δ = 1.19(2) mm s^{-1} and ΔE_Q = 2.90(2) mm s^{-1} that were obtained for a single quadrupole doublet are typical of high-spin iron(II) centers in a N/O coordination environment[45−47] and are comparable to those (δ = 1.3 mm s^{-1}; ΔE_Q = 2.4 − 3.13 mm s^{-1}) obtained for $MMOH_{red}$.[16b,31,48,49]

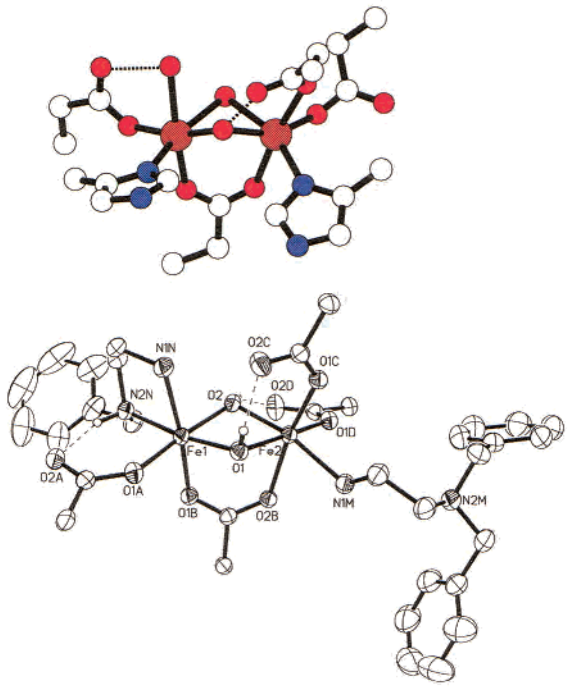

Figure 5. Ball-and-stick representation of the diiron(III) core structures of $MMOH_{ox}$ (top) and $[Fe_2(\mu\text{-}OH)_2(\mu\text{-}O_2CAr^{Tol})(O_2CAr^{Tol})_3(N\text{-Bnen})(N,N\text{-}Bn_2en)]$ (**8**) (bottom) generated using the crystallographic coordinates. For clarity, all atoms of the $Ar^{Tol}CO_2^-$ ligands in **8**, except for the carboxylate groups and the α-carbon atoms, were omitted.

Synthesis and Characterization of $[Fe_2(\mu\text{-}OH)_2(\mu\text{-}O_2CAr^{Tol})(O_2CAr^{Tol})_3(N\text{-Bnen})(N,N\text{-}Bn_2en)]$ (8).[31] Exposure of a colorless CH_2Cl_2 solution of **6** to dioxygen at room temperature resulted in a rapid color change to brownish yellow. Layering of pentanes over the solution afforded bright yellow blocks of **8** in modest yield (∼49%). The crystal structure of **8** is shown in Figure 5; selected bond lengths and angles are available in Table 3. Structural analysis of **8** revealed that one of the *N*,*N*-Bn_2en ligands in the precursor compound **6** was N-dealkylated to afford a new bidentate ligand *N*-Bnen[31] that was bound to Fe(1). The other *N*,*N*-Bn_2en ligand remained intact and was coordinated to Fe(2) in a monodentate fashion, as in **6**. The two iron atoms have pseudo-octahedral geometry and are linked by one carboxylate and two hydroxide ligands. The assignment of the single-atom bridging ligand as hydroxide is supported

(45) Kurtz, D. M., Jr. *Chem. Rev.* **1990**, *90*, 585.
(46) Gütlich, P.; Ensling, J. In *Inorganic Electronic Structure and Spectroscopy*; Solomon, E. I., Lever, A. B. P., Eds.; Wiley & Sons: New York, 1999; Vol. I, pp 161−211.
(47) Münck, E. In *Physical Methods in Bioinorganic Chemistry: Spectroscopy and Magnetism*; Que, L., Jr., Ed.; University Science Books: Sausalito, CA, 2000; pp 287−319.
(48) Fox, B. G.; Hendrich, M. P.; Surerus, K. K.; Andersson, K. K.; Froland, W. A.; Lipscomb, J. D.; Münck, E. *J. Am. Chem. Soc.* **1993**, *115*, 3688.
(49) Pulver, S.; Froland, W. A.; Fox., B. G.; Lipscomb, J. D.; Solomon, E. I. *J. Am. Chem. Soc.* **1993**, *115*, 12409.

Table 3. Selected Bond Lengths and Angles for **8**[a]

	Bond Length (Å)		Bond Angle (deg)
Fe(1)···Fe(1A)	2.9788(6)	O(1A)−Fe(1)−O(1)	92.85(7)
		O(1A)−Fe(1)−O(2)	173.12(7)
Fe(1)−O(1)	1.9726(17)	O(1)−Fe(1)−O(2)	80.27(7)
Fe(1)−O(2)	1.9977(17)	O(1A)−Fe(1)−O(1B)	87.61(7)
Fe(1)−O(1A)	1.9664(18)	O(1)−Fe(1)−O(1B)	93.05(7)
Fe(1)−O(1B)	2.0106(17)	O(2)−Fe(1)−O(1B)	92.67(7)
Fe(1)−N(1N)	2.151(2)	O(1A)−Fe(1)−N(1N)	91.20(8)
Fe(1)−N(2N)	2.172(2)	O(1)−Fe(1)−N(1N)	94.12(8)
Fe(2)−O(1)	1.9852(17)	O(2)−Fe(1)−N(1N)	89.36(8)
Fe(2)−O(2)	1.9805(16)	O(1B)−Fe(1)−N(1N)	172.78(8)
Fe(2)−O(2B)	2.1266(16)	O(1A)−Fe(1)−N(2N)	93.54(8)
Fe(2)−O(1C)	2.0045(17)	O(1)−Fe(1)−N(2N)	171.61(8)
Fe(2)−O(1D)	2.0171(17)	O(2)−Fe(1)−N(2N)	93.31(7)
Fe(2)−N(1M)	2.145(2)	O(1B)−Fe(1)−N(2N)	92.64(7)
		N(1N)−Fe(1)−N(2N)	80.32(8)
O(1)···O(2C)	2.681(3)	O(2)−Fe(2)−O(1)	80.39(7)
O(2)···O(2D)	2.668(3)	O(2)−Fe(2)−O(1C)	100.97(7)
N(2N)···O(2A)	2.891(3)	O(1)−Fe(2)−O(1C)	92.40(7)
		O(2)−Fe(2)−O(1D)	93.50(7)
		O(1)−Fe(2)−O(1D)	172.43(7)
		O(1C)−Fe(2)−O(1D)	93.16(7)
		O(2)−Fe(2)−O(2B)	90.35(7)
		O(1)−Fe(2)−O(2B)	85.53(7)
		O(1C)−Fe(2)−O(2B)	168.00(7)
		O(1D)−Fe(2)−O(2B)	90.07(7)
		O(2)−Fe(2)−N(1M)	167.69(8)
		O(1)−Fe(2)−N(1M)	96.70(8)
		O(1C)−Fe(2)−N(1M)	91.06(8)
		O(1D)−Fe(2)−N(1M)	88.34(8)
		O(2B)−Fe(2)−N(1M)	77.48(7)

[a] Numbers in parentheses are estimated standard deviations of the last significant figure. Atoms are labeled as indicated in Figure 5.

by the Fe−O distances, which range from 1.9726(17) to 1.9977(17) Å, as well as by the location and refinement of the associated hydrogen atoms in the X-ray structure determination. Comparable Fe−$O_{hydroxo}$ distances exist in other high-spin iron(III) complexes having $\{Fe_2(\mu\text{-}OH)_2\}^{4+}$ core fragments.[23,24,50,51] The triply bridged diiron(III) core in **8** is further stabilized by hydrogen-bonding interactions in the second coordination sphere (Figure 5). Specifically, the three nonbridging carboxylate ligands are hydrogen-bonded to the bridging hydroxides or to the newly derived secondary amine group on the *N*-Bnen ligand, with $O_{carboxylate}$···X (X = $O_{hydroxide}$ or N_{amine}) distances ranging from 2.668(3) to 2.891(3) Å. The Fe···Fe distance of 2.9788(6) Å is shorter than those (3.089(2)−3.155(3) Å) in the doubly bridged $\{Fe_2(\mu\text{-}OH)_2\}^{4+}$ cores[50,51] but longer than those (2.8322(8)−2.8843(9) Å) in the quadruply bridged $\{Fe_2(\mu\text{-}OH)_2(\mu\text{-}O_2CAr^{Tol})_2\}^{2+}$ cores.[23,24]

Except for a shoulder at ∼330 nm, the UV−vis spectra of **8** (Figure S3) are rather featureless and do not display any longer-wavelength LMCT transitions. These properties are consistent with the presence of hydroxo, not oxo, bridging ligands.[2e,45] The Mössbauer spectrum obtained for a solid sample of **8** at 77 K (Figure S4) exhibits a broad (Γ = 0.62−0.74 mm s^{-1}) asymmetric quadrupole doublet that is indicative of paramagnetic relaxation. At 4.2 K, a narrower (Γ = 0.33−0.35 mm s^{-1}) well-resolved single quadrupole doublet was obtained (Figure 6), which was fit with δ = 0.48(2) mm s^{-1} and ΔE_Q = 0.61(2) mm s^{-1}. These parameters are typical for high-spin iron(III) centers with pseudo-octahedral geometry.[45−47] The narrow peak width indicates that the two iron atoms in **8** are indistinguishable under the Mössbauer conditions.

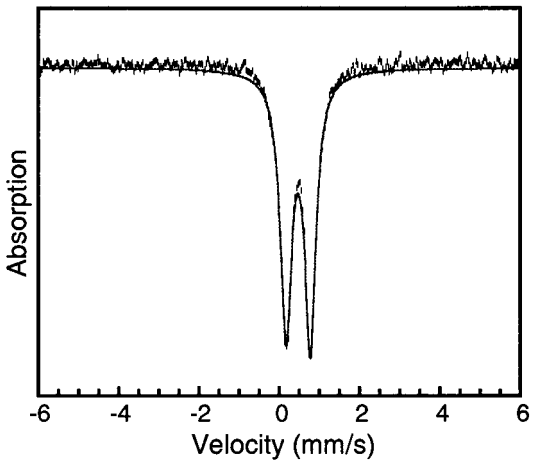

Figure 6. Zero-field Mössbauer spectrum (experimental data (|), calculated fit (−)) recorded at 4.2 K for $[Fe_2(\mu\text{-}OH)_2(\mu\text{-}O_2CAr^{Tol})(O_2CAr^{Tol})_3(N\text{-Bnen})(N,N\text{-}Bn_2en)]$ (**8**) in the solid state. See text for derived Mössbauer parameters.

Oxidative N-Dealkylation. Following exposure of CH_2Cl_2 solutions of **6** to dioxygen at room temperature, the reaction mixture was analyzed. GC−MS studies revealed the formation of PhCHO in an average yield of 60(5)% based on [Fe_2]. The origin of the oxygen atom incorporated into PhCHO was established by use of $^{18}O_2$, which afforded PhCH^{18}O as the major isotopomer (90:10 PhCH^{18}O/PhCH^{16}O) under similar conditions. This result provides compelling evidence that the *N*-Bnen ligand in **8** is the product of oxidative N-dealkylation of **6**. Insertion of an O_2-derived oxygen atom into the benzylic C−H bond affords the α-hydroxylamine, which decomposes to the final products, the dealkylated amine and PhCHO. This process is well-documented for cP450[2d,52] as well as for copper dioxygen chemistry.[4,6,53−57] Upon prolonged exposure to air, the labeled oxygen atom of PhCH^{18}O in the reaction mixture is exchanged. We suspect that the small amount of PhCH^{16}O identified in the reaction mixture may result from the reaction of PhCH^{18}O with trace amounts of H_2O that are introduced during sample handling.

When a noncoordinating analogue of *N*,*N*-Bn_2en such as *N*,*N*-dibenzylpropylamine was employed as an external

(50) Thich, J. A.; Ou, C. C.; Powers, D.; Vasiliou, B.; Mastropaolo, D.; Potenza, J. A.; Schugar, H. J. *J. Am. Chem. Soc.* **1976**, *98*, 1425.
(51) Borer, L.; Thalken, L.; Ceccarelli, C.; Glick, M.; Zhang, J. H.; Reiff, W. M. *Inorg. Chem.* **1983**, *22*, 1719.
(52) Silverman, R. B. *The Organic Chemistry of Enzyme-Catalyzed Reactions*; Academic Press: San Diego, CA, 2000.
(53) Mahapatra, S.; Halfen, J. A.; Wilkinson, E. C.; Pan, G.; Wang, X.; Young, V. G., Jr.; Cramer, C. J.; Que, L., Jr.; Tolman, W. B. *J. Am. Chem. Soc.* **1996**, *118*, 11555.
(54) Mahapatra, S.; Halfen, J. A.; Tolman, W. B. *J. Am. Chem. Soc.* **1996**, *118*, 11575.
(55) Mahapatra, S.; Young, V. G., Jr.; Kaderli, S.; Zuberbühler, A. D.; Tolman, W. B. *Angew. Chem., Int. Ed. Engl.* **1997**, *36*, 130.
(56) Mahadevan, V.; Hou, Z.; Cole, A. P.; Root, D. E.; Lal, T. K.; Solomon, E. I.; Stack, T. D. P. *J. Am. Chem. Soc.* **1997**, *119*, 11996.
(57) Mahadevan, V.; Henson, M. J.; Solomon, E. I.; Stack, T. D. P. *J. Am. Chem. Soc.* **2000**, *122*, 10249.

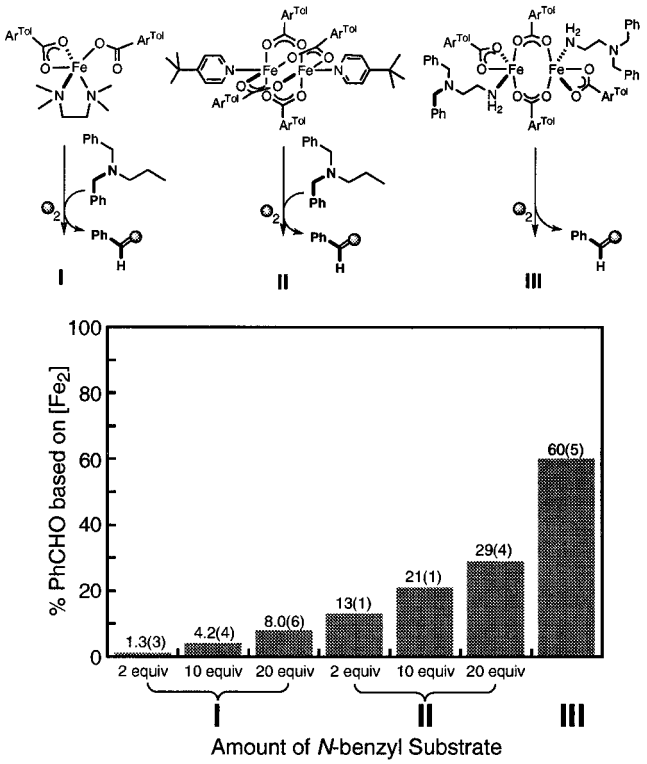

Figure 7. Oxidative N-dealkylation of internal versus external amine substrates by mono- and dinuclear iron(II) complexes.

substrate in conjunction with either a mononuclear or a dinuclear iron(II) complex, the yield of the N-dealkylation product was significantly reduced. Under reaction conditions similar to those used for **6** (2 equiv of amine substrate per Fe^{II}_2), $[Fe(O_2CAr^{Tol})_2(TMEDA)]$[31,32] afforded only 1.3(3)% and $[Fe_2(\mu\text{-}O_2CAr^{Tol})_4(4\text{-}^tBuC_5H_4N)_2]$[24], 13(1)% of PhCHO. Even with a 10-fold increase in the substrate loading, the efficiency of the external substrate oxidation is significantly lower than that effected by **6** (Figure 7).

Discussion

Synthetic Routes to Diiron(II) Complexes. A range of bidentate N-donor ligands was screened to implement strategy **II** in Scheme 2. Initial attempts to install bidentate ligands into the preassembled diiron(II) module $\{Fe_2(\mu\text{-}O_2CAr^{Tol})_2(O_2CAr^{Tol})_2\}$ resulted in unwanted core disassembly to mononuclear species. For example, sterically demanding diamine ligands such as TMEDA[31] or diamine ligands that have smaller bite angles such as 3-dimethylaminopropylamine afforded five- or six-coordinate monoiron(II) complexes (Scheme 3).[29] By proper choice of the diamine ligand, the desired dinuclear complex **2** was obtained, but only in a mixture that also contained **3** and **4**, which can be regarded as formal disproportionation products of **2**. A more sterically demanding *N*,*N*-disubstituted ethylenediamine was thus targeted.

In the design of this new ligand, we also intended to integrate potential substrate fragments as part of the ethylenediamine derivative. By juxtaposing oxidizable C−H bonds with the reactive metal−dioxygen adduct, we planned to achieve the desired functional chemistry using enzyme models that lack substrate binding cavities. A similar strategy has been previously adopted for related copper oxidation chemistry[4,6,53−59] as well as for metallohydrolase models.[60,61] We therefore introduced the *N*,*N*-Bn_2en diamine ligand in the synthesis of the diiron(II) complexes. The more sterically demanding benzyl groups installed on the nitrogen atom effectively blocked the formation of the undesired bis(chelate) complexes, affording analytically pure diiron(II) compounds **5**−**7**. The primary coordination spheres of **6** and **7** comprise four carboxylate ligands and two N-donor ligands, just like the diiron(II) center in $MMOH_{red}$ and in related proteins.[2a,c,e,14,15,62]

Structural Model of $MMOH_{ox}$. Among several crystal structures of $MMOH_{ox}$[31] determined under different conditions,[62−68] two examples feature the $\{Fe_2(\mu\text{-}OH)_2(\mu\text{-}O_2CR)\}^{3+}$ dimetallic core (Figure 5),[62,66] which previously has not been reproduced outside the enzyme environment. Analogous $\{M_2(\mu\text{-}OH)_2(\mu\text{-}O_2CR)\}^{3+}$ units exist in kinetically inert dichromium(III),[69] dimolybdenum(III),[70] dicobalt(III),[71] and diruthenium(III)[72] complexes. A survey of the CSD revealed that triply bridged $\{Fe_2(\mu\text{-}X)(\mu\text{-}O_2CR)_2\}^{n+}$ cores comprising a single atom bridge (X = OH^- or OR^-) and two μ-1,3 bridging carboxylate ligands are preferred by diiron complexes (**C**, Scheme 4). The steric hindrance imposed by the *p*-tolyl substituents on the $Ar^{Tol}CO_2^-$ ligand may preclude coordination of two bridging carboxylate ligands in the orthogonal positions. As a result, only one carboxylate ligand can be accommodated in the triply bridged core in **8** (**D**, Scheme 4). Alternatively, two bridging $Ar^{Tol}CO_2^-$ ligands can be arranged trans across the $\{Fe_2(\mu\text{-}OH)_2\}^{4+}$ plane, as in $[Fe_2(\mu\text{-}OH)_2(\mu\text{-}O_2CAr^{Tol})_2(O_2CAr^{Tol})_2L_2]$[23,24] where L = C_5H_5N or 4-$^tBuC_5H_4N$ (**E**, Scheme 4). This configuration, however, is not allowed for **8**, owing to the bidentate *N*-Bnen ligand that occupies the axial position of Fe(1) (Figure 5).

(58) Itoh, S.; Taki, M.; Nakao, H.; Holland, P. L.; Tolman, W. B.; Que, L., Jr.; Fukuzumi, S. *Angew. Chem., Int. Ed.* **2000**, *39*, 398.
(59) Zhang, C. X.; Liang, H.-C.; Kim, E.-I.; Gan, Q.-F.; Tyeklár, Z.; Lam, K.-C.; Rheingold, A. L.; Kaderli, S.; Zuberbühler, A. D.; Karlin, K. D. *Chem. Commun.* **2001**, 631.
(60) He, C.; Lippard, S. J. *J. Am. Chem. Soc.* **1998**, *120*, 105.
(61) Barrios, A. M.; Lippard, S. J. *J. Am. Chem. Soc.* **1999**, *121*, 11751.
(62) Whittington, D. A.; Lippard, S. J. *J. Am. Chem. Soc.* **2001**, *123*, 827.
(63) Rosenzweig, A. C.; Frederick, C. A.; Lippard, S. J.; Nordlund, P. *Nature* **1993**, *366*, 537.
(64) Rosenzweig, A. C.; Lippard, S. J. *Acc. Chem. Res.* **1994**, *27*, 229.
(65) Rosenzweig, A. C.; Nordlund, P.; Takahara, P. M.; Frederick, C. A.; Lippard, S. J. *Chem. Biol.* **1995**, *2*, 409.
(66) Elango, N.; Radhakrishnan, R.; Froland, W. A.; Wallar, B. J.; Earhart, C. A.; Lipscomb, J. D.; Ohlendorf, D. H. *Protein Sci.* **1997**, *6*, 556.
(67) Whittington, D. A.; Sazinsky, M. H.; Lippard, S. J. *J. Am. Chem. Soc.* **2001**, *123*, 1794.
(68) Whittington, D. A.; Rosenzweig, A. C.; Frederick, C. A.; Lippard, S. J. *Biochemistry* **2001**, *40*, 3476.
(69) (a) Fujihara, T.; Fuyuhiro, A.; Kaizaki, S. *Inorg. Chim. Acta* **1998**, *278*, 15. (b) Toftlund, H.; Simonsen, O.; Pedersen, E. *Acta Chem. Scand.* **1990**, *44*, 676.
(70) (a) Wieghardt, K.; Hahn, M.; Swiridoff, W.; Weiss, J. *Inorg. Chem.* **1984**, *23*, 94. (b) Kneale, G. G.; Geddes, A. J. *Acta Crystallogr., Sect. B* **1975**, *31*, 1233.
(71) (a) Dimitrou, K.; Folting, K.; Streib, W. E.; Christou, G. *J. Am. Chem. Soc.* **1993**, *115*, 6432. (b) Sumner, C. E., Jr. *Inorg. Chem.* **1988**, *27*, 1320. (c) Mandel, G. S.; Marsh, R. E.; Schaefer, W. P.; Mandel, N. S. *Acta Crystallogr., Sect. B* **1977**, *33*, 3185. (d) Maas, G. *Z. Anorg. Allg. Chem.* **1977**, *432*, 203.
(72) Wieghardt, K.; Herrmann, W.; Köppen, M.; Jibril, I.; Huttner, G. *Z. Naturforsch., B: Chem. Sci.* **1984**, *39*, 1335.

Scheme 4

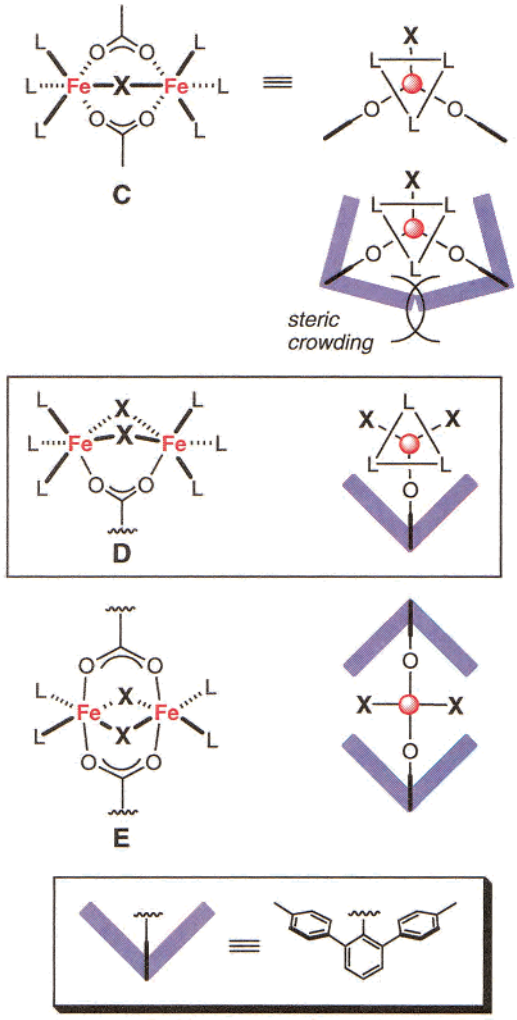

Taken together, the unique structural requirements of the bulky $Ar^{Tol}CO_2^-$ and *N*-Bnen ligands play an essential role in assembling the biomimetic $\{Fe_2(\mu\text{-}OH)_2(\mu\text{-}O_2CR)\}^{3+}$ core outside the well-structured four-helix bundle scaffold[73] of the enzyme.

Both iron atoms in $MMOH_{ox}$ from *Methylosinus trichosporium* OB3b have a distorted octahedral coordination environment.[66] The metal···metal distance of 2.99 Å is spanned by one carboxylate and two hydroxide bridging ligands, with $Fe-O_{hydroxide}$ distances of 1.71−2.17 Å. The Fe···Fe and $Fe-O_{hydroxide}$ distances of 2.9788(6) and 1.9726(17)−1.9977(17) Å, respectively, in **8** support the assignment of the single-atom bridging ligands in the enzyme as hydroxide groups. A significantly increased metal···metal distance of 3.2 Å was obtained for $MMOH_{ox}$ that was isolated from *Methylococcus capsulatus* (Bath), for which one of the single-atom bridging ligands was modeled as a weakly bound $H_3O_2^-$ ion.[62] In both structures, two histidine and three carboxylate terminal ligands, along with solvent-derived molecules, complete the NO_5 donor-atom sets for each metal.

A slightly different ligand combination is adopted by **8**, which has a N_2O_4 set for one iron atom and a NO_5 set for the other iron atom. Hydrogen-bonding interactions in the second coordination sphere apparently strengthen the dimetallic core in **8**. Notably, the hydrogen-bonding interaction between the axial carboxylate ligands and one of the bridging hydroxide ligands also occurs in $MMOH_{ox}$ from *M. capsulatus* (Bath).[62]

Zero-field Mössbauer spectra obtained at 4 K for $MMOH_{ox}$ from *M. capsulatus* (Bath) indicated the presence of two slightly nonequivalent high-spin iron(III) sites in a 1:1 ratio.[16b] Comparable sets of parameters were obtained for the spectra of $MMOH_{ox}$ from *M. trichosporium* OB3b, which were similarly modeled as the sum of two quadrupole doublets.[48] As indicated in Table 4, the isomer shift parameter of **8** is comparable to those of $MMOH_{ox}$ and a structurally related diiron(III) complex $[Fe_2(\mu\text{-}OH)_2(\mu\text{-}O_2CAr^{Tol})_2(O_2CAr^{Tol})_2(4\text{-}^tBuC_5H_4N)_2]$.[16b,48,74] The significantly different ΔE_Q values obtained for **8** and $[Fe_2(\mu\text{-}OH)_2(\mu\text{-}O_2CAr^{Tol})_2(O_2CAr^{Tol})_2(4\text{-}^tBuC_5H_4N)_2]$, both having six-coordinate iron atoms, however, are somewhat unexpected. Deviations from idealized O_h geometry increase the ΔE_Q values for a high-spin d^5 systems, whereas the δ values are barely influenced by such variations. The two nonequivalent iron sites identified for the $MMOH_{ox}$ core (Table 4) may reflect such a subtle structural modification in coordination geometry.

Mechanism of Oxidative N-Dealkylation. Although detailed information about the conversion of **6** to **8** is currently unavailable, we postulate the mechanism depicted in Scheme 5.[75] This working hypothesis is based upon mechanistic frameworks previously developed to explain similar chemical transformations effected by cP450[2d,52] or copper amine complexes.[54] In these systems, high-valent iron(IV)−oxo porphyrin π-radical or di(μ-oxo)dicopper(III) species were invoked as reactive intermediates that first hydroxylate the C−H bonds α to the nitrogen, affording the corresponding aldehyde or ketone as the final products.

In this work, we postulate the involvement of a reactive dioxygen adduct of **6** either at the (peroxo)diiron(III) or di(oxo)diiron(IV) oxidation level, by analogy to the MMOH reaction cycle.[2a,c,e,14] Given the fundamentally nucleophilic nature of well-characterized (peroxo)diiron(III) species supported on tetracarboxylate ligand frameworks,[76,77] we consider the di(oxo)diiron(IV) species to be the functionally competent unit. A high-valent iron(IV) oxo species has also been implicated in the catalytic cycle of the mononuclear iron(II) complex $[L^1Fe(MeCN)_2]^{2+}$ [31] that, in conjunction with H_2O_2, catalyzes oxidative N-dealkylation, stereoselective alkane hydroxylation, and olefin epoxidation.[78] The electro-

(73) Lombardi, A.; Summa, C. M.; Geremia, S.; Randaccio, L.; Pavone, V.; DeGrado, W. F. *Proc. Natl. Acad. Sci. U.S.A.* **2000**, *97*, 6298.

(74) Lee, D.; Pierce, B.; Krebs, C.; Hendrich, M. P.; Huynh, B. H.; Lippard, S. J. Submitted for publication.

(75) This mechanism assumes monooxygenase activity, by which only one oxygen atom from O_2 is transferred to the substrate. Dioxygenase activity, for which one molecule of O_2 would afford two PhCHO components, cannot be formally excluded, however.

(76) LeCloux, D. D.; Barrios, A. M.; Mizoguchi, T. J.; Lippard, S. J. *J. Am. Chem. Soc.* **1998**, *120*, 9001.

(77) LeCloux, D. D.; Barrios, A. M.; Lippard, S. J. *Bioorg. Med. Chem.* **1999**, *7*, 763.

Table 4. Mössbauer Parameters of the Diiron(III) Centers in $MMOH_{ox}$, $[Fe_2(\mu\text{-}OH)_2(\mu\text{-}O_2CAr^{Tol})(O_2CAr^{Tol})_3(N\text{-Bnen})(N,N\text{-}Bn_2En)]$ (**8**), and $[Fe_2(\mu\text{-}OH)_2(\mu\text{-}O_2CAr^{Tol})_2(O_2CAr^{Tol})_2(4\text{-}^tBuC_5H_4N)_2]$ Measured at 4 K

	δ (mm/s)	ΔE_Q (mm/s)		ref
$MMOH_{ox}$ (*M. capsulatus* (Bath))	0.51(2)	1.12(3)	site 1	16b
	0.50(2)	0.79(3)	site 2	
$MMOH_{ox}$ (*M. trichosporium* OB3b)	0.51	1.16	site 1	48
	0.50	0.87	site 2	
8	0.48(2)	0.61(2)		this work
$[Fe_2(\mu\text{-}OH)_2(\mu\text{-}O_2CAr^{Tol})_2(O_2CAr^{Tol})_2(4\text{-}^tBuC_5H_4N)_2]$	0.49(2)	1.01(2)		74

Scheme 5

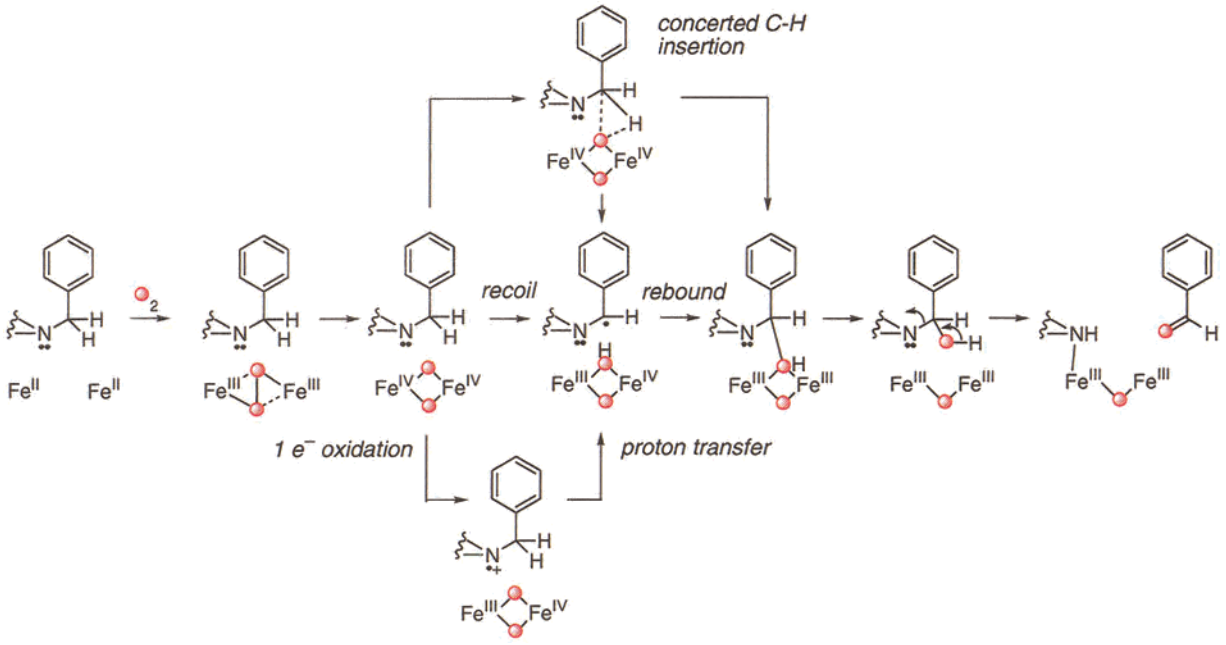

philic nature of the $\{Cu_2(\mu\text{-}O)_2\}^{2+}$ center, which effects α-hydroxylation of the metal-bound alkylamine ligand, is also well-established.[54]

Insertion of the oxygen atom into the benzylic C−H bond of *N,N*-Bn_2en can proceed by at least three distinguishable reaction pathways. Conventional recoil with hydrogen atom transfer (middle, Scheme 5) or sequential single-electron transfer (SET), deprotonation, and internal electron transfer (bottom, Scheme 5) can equally well provide the α-carbon-centered neutral radical. Subsequent oxygen rebound affords the α-hydroxylamine. Alternatively, concerted insertion of the oxygen atom into the C−H bond can be invoked (top, Scheme 5). In the key C−H bond activation step, the tertiary amine group of the *N,N*-Bn_2en ligand may remain coordinated to the metal center, as in **5**. In such an event, the coupled Fe(III) aminium cation radical in the SET pathway can be alternatively formulated as an Fe(IV) amine. The SET pathway is implicated in cP450-catalyzed oxidative N-dealkylation,[2d] whereas direct intramolecular attack at the C−H bond is favored for the di(μ-oxo)dicopper(III) system.[54] Efforts are currently in progress to delineate the mechanism of oxidative N-dealkylation effected by the present non-heme diiron model systems.

(78) Mekmouche, Y.; Ménage, S.; Toia-Duboc, C.; Fontecave, M.; Galey, J.-B.; Lebrun, C.; Pécaut, J. *Angew. Chem., Int. Ed.* **2001**, *40*, 949.

Summary and Perspective

Synthetic routes were developed to install potential substrates into ligand fragments bound to non-heme diiron(II) model complexes. Reaction of one such compound with O_2 effected the unprecedented oxidative N-dealkylation of a benzylamine fragment. The reaction also afforded the first diiron(III) complex having the $\{Fe_2(\mu\text{-}OH)_2(\mu\text{-}O_2CR)\}^{3+}$ core structure of $MMOH_{ox}$, which previously has not been replicated outside the enzyme. A well-defined synthetic module is now accessible, the elaboration of which will significantly extend the scope of structure−function studies that can be carried out with dioxygen-activating non-heme diiron(II) models. The reaction coordinates mapped by such complexes should help to unravel the details of biological C−H activation at the molecular level.

Acknowledgment. This work was supported by grants from the National Science Foundation and the National Institute of General Medical Sciences. We thank Ms. Jane Kuzelka for help in acquiring the Mössbauer spectra.

Supporting Information Available: Figures S1 and S2 showing ORTEP diagrams of **3** and **4**, physical characterization of **8** (Figures S3 and S4), and an X-ray crystallographic file (CIF). This material is available free of charge via the Internet at http://pubs.acs.org.

IC011008S